Photocatalytic Activity of Titanium Dioxide Modified by Silver Nanoparticles

Dawid Wodka,*,† Elżbieta Bielańska,† Robert P. Socha,† Magdalena Elżbieciak - Wodka,† Jacek Gurgul,† Paweł Nowak,† Piotr Warszyński,† and Izumi Kumakiri‡

Institute of Catalysis and Surface Chemistry, Polish Academy of Sciences, 30-239 Krakow, Poland, and Materials and Chemistry, The Foundation for Scientific and Industrial Research (SINTEF), P.O. Box 124 Blindern, 0314 Oslo, Norway

ABSTRACT Photocatalytic activity of Ag/TiO_2 composites obtained by photoreduction treatment (PRT) was investigated. The composite materials, containing various ratio of silver nanoparticles (0.6−3.7 wt %) were obtained by depositing silver on the Evonic-Degussa P25 titania surface. Selected samples whose color varied between light rose and purple brown were examined by SEM, TEM, XPS, DRS, and BET techniques. Flat band potential was determined using Roy method. TEM analysis showed spherically shaped silver nanoparticles of the diameter 4−12 nm. The XPS measurements revealed that silver particles were obtained mainly in metallic form. DRS spectra and photovoltage measurements showed that silver nanoparticles modified the P25 spectral properties but they changed neither the band gap nor the location of flat band potential. The photocatalytic activity of Ag/P25 composite was compared to the photocatalytic activity of pure P25 in the photooxidation reaction of an important potable water contaminant humic acid (HA) and two model compounds, oxalic acid (OxA) and formic acid (FA). The photodecomposition reaction was investigated in a batch reactor containing aqueous suspension of a photocatalyst illuminated by either UV or artificial sunlight (halogen lamp). The tests proved that a small amount of silver nanoparticles deposited on the titania surface triggers the increase in photocatalytic activity; this increase depends, however, on the decomposed substance.

KEYWORDS: titanium dioxide • photocatalysis • silver nanoparticles • water purification • humic substances

INTRODUCTION

Heterogeneous photocatalysis is an economically alternative and environmentally safe technology of advanced oxidation processes (AOP) for removal of organic impurities from water. During that process, the semiconductor illuminated by light of the proper wavelength absorbs light and generates active species, which oxidize the organic compounds dissolved in water. The most popular and promising material for this application is TiO_2 because of its high physical and chemical stability, nontoxicity, and low price (1). However, its main drawbacks of low quantum yield and limited photoresponse range ($\lambda < 380$ nm) hinder its application and commercialization (2). To handle those problems, researchers have adopted numerous strategies, including phase and morphological control, doping, sensitizations, and semiconductor coupling (1−14). Recently, there has been a great interest in the photoelectrochemical properties of nanostructured TiO_2 films such as photovoltaic (15, 16), photocatalytic (17), optical (18), and water splitting ability (19). Several researchers reported that modification of the TiO_2 surface with metals like Pt, Fe, Ag, Au, and Pd is promising as a tool to enhance the photocatalytic activity of TiO_2 and to increase the quantum yield (20−23). In particular, silver nanoparticles deposited on TiO_2 substrate (Ag/TiO_2) have attracted significant attention because of nontoxicity of this metal with remarkable catalytic and antibacterial activity (24−30). Moreover, silver is particularly suitable for industrial applications because of its relatively low price and the ease of the Ag/TiO_2 composite preparation when compared to other metals. Activity of those materials has been tested with many organic compounds like organic dyes (31, 32), phenols, ketones (25), carboxylic acids (33) in solid−liquid as well as in solid−gas systems. In those kinds of reactions, the Ag/TiO_2 composite showed usually higher activity than bare titania. The most common and promising methods of preparation of Ag/TiO_2 composites, which make possible approaching the systems of high efficiency and low cost are sol−gel (34, 35), PRT (36, 37), and CVD (38) ones.

The aim of this work was the optimization of the preparation procedure of Ag/TiO_2 composites by using organic metal basis in PRT reaction and minimizing the diameter of Ag particles. The composites were synthesized from organic silver salt (silver acetate). The application of acetate in the PRT reaction allowed synthesizing metallic nanoparticles without any additional reducer. In such photoreaction process, the organic anion (sacrificial reagent) causes reduction of silver cations to the metallic state. It makes that kind of synthesis simple, fast, and relatively cheap, and makes it possible to obtain pure composites without any impurities, which is a big advantage when compared to reduction of $AgNO_3$ (39−41). The Ag/TiO_2 photocatalysts containing silver particles were tested in the decomposition of selected organic compounds like oxalic acid (OxA), formic acid (FA), and humic acid (HA) (42). Results recorded for silver modified titania were compared to pure P25.

* Corresponding author.
Received for review March 26, 2010 and accepted June 10, 2010
† Polish Academy of Sciences.
‡ The Foundation for Scientific and Industrial Research (SINTEF).
DOI: 10.1021/am1002684

In this paper, we take special note of potential applications of the investigated materials for environmental pollutant elimination from water potentially connected with the photoinduced elimination of micro-organisms. So, the activity of obtained photocatalysts was tested with the natural contaminant, humic acid (HA), which appears frequently in natural waters. That species is a significant component of humic substances derived from the decomposition of plant and animal matter (43). It is a complex mixture of organic compounds hardly removable in the water treatment processes. The presence of humic substances can impart an undesirable taste and color to drinking water, which forces the search for highly effective methods for removing those kinds of contaminations (44).

EXPERIMENTAL SECTION

Materials and Reagents. TiO_2 (P25, 25% rutile and 75% anatase) was kindly supplied by Evonic-Degussa. Silver acetate 99.99% metals basis, barium sulfate ((ReagentPlus, 99%), and humic acid sodium salt (technical grade) were purchased form Sigma-Aldrich. Other reagents were obtained from POCh Gliwice, Poland (oxalic acid (OxA) 99.5%, p.a., potassium manganate (VII) (99.0%, p.a.), potassium thiocyanate (99.0%, p.a.), nitric acid (65.0%, p.a), sodium carbonate (anhydrous, 99.8% p.a.), silver nitrate (p.a), and sulfuric acid (≥95.0%, p.a.)), and Fluka (formic acid (FA) 98.0% p.a.). Solution of humic acid was made from Sigma-Aldrich technical HA sodium salt and used after filtration (0.45 μm) and centrifugation (12.000 rpm for 30 min) to remove coarse particles. Methylviologen hexafluorophosphate was kindly supplied by Jagiellonian University, Department of Chemistry. All reagents were used as received without further purification. Deionized water of Millipore Direct Q UV quality was used in all experiments.

Preparation of Ag/TiO_2. The Ag/TiO_2 nanocomposites were obtained by a photoreduction treatment (PRT). The composite suspension (40 mL) was prepared by mixing P25 powder (1 g) with different volumes of CH_3COOAg aqueous solution (0.05 M) and deionized water. The suspension was then sonificated for 10 min, and finally agitated (300 rpm) and irradiated with a high-pressure xenon arc lamp (250 W) for 1 h in a quartz flat bottomed cell. The resulting Ag/TiO_2 nanocomposite was recovered by filtration, rinsed with deionized water several times, and finally, dried at 40 °C in the dark. The composites were prepared for following Ag/TiO_2 ratios in the synthesis mixture (%): 1, 2, 3, 5, 10, 20, and 30. The determination of real silver concentration in composite was done by dissolving silver from the composite in nitric acid and titration using the Volhard method. In the further text, the real concentration of silver, presented in wt %, is given.

Material Characterization. The scanning electron microscopy (SEM) images and EDXS analysis were performed with a JEOL JSM-7500F field-emission apparatus operated at 15 kV. The samples were analyzed without any surface treatment.

The TECNAI G2 instrument equipped with EDXS system was used for transmission electron microscopy (TEM) investigations. Apparatus was operated at 200 kV.

The X-ray photoelectron spectroscopy (XPS) and X-ray excited Auger electron spectroscopy (XAES) measurements were performed using an XPS spectrometer equipped with a hemispherical analyzer (R4000, Gammadata Scienta) and MgKα (1253.6 eV) radiation. The power of the X-ray source was 240 W and the analyzer pass energy was 100 eV, corresponding to a full width at half-maximum (fwhm) of 0.9 eV for the Ag $3d_{5/2}$ peak. The area of the analyzed sample was approximately 3 mm^2. The powder samples were pressed into indium foil and mounted on a dedicated holder. In the case of Ag/TiO_2 suspensions, the drop of liquid sample was dried at the gold sheet surface and then analyzed. The binding energy (BE) was calibrated using Cu, Au, and Ag foils as reference materials, according to the ISO 15472:2001 procedure.

DRS measurements were performed with a Perkin-Elmer Lambda 35 spectrometer provided with a diffuse reflectance accessory. Photocatalysts were diluted with $BaSO_4$ (10 mg of photocatalyst and 1 g of $BaSO_4$) and ground in an agate mortar. Subsequently, 10 mm pellets were prepared for the analysis. The background reflectance of $BaSO_4$ was measured first. Spectra were registered in the 190−1100 nm range with 240 nm/min scan speed.

Flat band potential was determined using the Roy method (45). Setup was assembled with a thermostatted flat-bottomed cell made from Pyrex glass. A 1 cm^2 Pt foil electrode was used as a working electrode and Ag/AgCl/sat.KCl electrode as the reference electrode. A combined glass electrode was used for pH measurement. All these electrodes were inserted through the Plexiglas lid covering the cell. pH was adjusted by means of an infusion pump (TSE systems NE-1000) with 0.1 M Na_2CO_3 after suspension acidification by concentrated sulfuric acid. One-hundred milligrams of of semiconductor powder was placed in the cell and 100 mL of 0.1 M KNO_3 was added. Then suspension was sonificated for 15 min and the mixture was purged from oxygen by intensive bubbling with laboratory grade Ar (Linde) for 15 min, and then 20 mg of methylviologen was added. The mixture was again bubbled with argon for 10 min. During the measurement suspension was irradiated with 250 W xenon arc lamp, stirred with mechanical stirrer and continuously bubbled with Ar. The potential of the working electrode was recorded with a Brymen BM857 multifunction meter. An Elmetron CX-401 multifunction meter was used for pH measurements.

The cyclic voltammetry (CV) measurements were carried out using PGSTAT302N potentiostat/galvanostat (Autolab). Glass cell with Pt foil counter electrode, Ag/AgCl/sat.KCl electrode as the reference electrode and Pt wire as a working electrode was used in the measurements. Solutions were purified from oxygen by bubbling with laboratory grade argon (Linde) for 15 min before measurements. The CV measurements were performed at the sweep rate of 100 mV/s and 0.1 M KNO_3 was used as a base electrolyte.

The Brunauer−Emmett−Teller (BET) surface area of the powder samples was determined with a QuantaChrome Autosorb-1 instrument. The surface area of the samples was obtained from nitrogen adsorption isotherms after outgassing for 18 h at the temperature of 20 °C.

Photodegradation Experiments. The photooxidation experiments were performed in two identical quartz flat bottomed batch reactors of the volume 40 mL. In the first reactor, a halogen lamp (150 W, Philips) was used as the artificial sunlight (ASL) source; in the other one, dedicated for ultraviolet (UV), the high-pressure xenon arc lamp (250 W, Optel) was applied. Both lamps were used without any cutoff filters, except the layer of cooling water flowing below the bottom of the cell. The cell illumination was monitored by the radiometer Radiometer RD 0.2/2/100 (Optel). In those measurements sensor was placed at the top of the empty reactor. The distance between the source and the sensor was about 25 cm for ASL and 15 cm for UV light and the illumination area was 16.3 cm^2. The irradiation intensity was 68.8 mW/cm^2 for ASL and 48.8 mW/cm^2 for UV source. The photocatalyst suspensions were stirred during the experiments in both reactors with a mechanical stirrer at a constant rate of 300 rpm. A mechanical stirrer with the stirring rod positioned a few millimeters above the bottom of the cell was used instead of a magnetic stirrer to avoid grinding of the TiO_2 grains during the measurement. The temperature was stabilized at 25 ± 0.5 °C (see Figure I in the Supporting Information).

Table 1. Parameters of the Photodegradation Experiments

contaminant	OxA	FA	HA
$C_{contaminant}$	5×10^{-4} M	4×10^{-2} M	40 mg/L
$C_{photocatalyst}$ (mg/L)	500	500	100
irradiation time (min)	5, 20	60	60
analytical wavelength (nm)	195	208	254

Together with the sample used in a photocatalytic experiment, an identical reference sample was prepared and kept in the dark during the same period of time. After the experiment, three portions of both suspension and reference samples were taken, subjected to 25 min of centrifugation at 15 000 rpm to separate TiO_2, and then analyzed for the contaminant concentration. In that way, the influence of adsorption on the TiO_2 surface on the uptake of the contaminant from the solution was eliminated. The concentration changes of different contaminants were determined by UV−vis spectrophotometery (Specord 40, Analytik Jena). The most characteristic wavelength of maximum light absorption was chosen for all contaminants. After preliminary experiments, the following photocatalyst and contaminant concentrations as well as irradiation times were chosen for testing the activity of the Ag/TiO_2 composites, as shown in Table 1.

The initial contaminant concentrations were selected to fit the optimum spectrophotometer absorbance range of 1.0−2.0. The percentage of the decomposed contamination was calculated using following eq 1

$$\%_{decomp} = \frac{(A_0 - A)}{A_0} 100\ (\%) \qquad (1)$$

where A_0 is absorbance of the reference sample and A is the suspension absorbance after irradiation.

Sample preparation to the spectrophotometric measurement is schematically showed in Figure 1. Stability of investigated compounds versus decomposition under the influence of irradiation was checked in blank experiments without the photocatalyst. After 3 h of illumination under ASL and UV light, the photodecomposition effect was negligibly small for all used substrates.

The usefulness of spectrophotometery to the determination of the oxalic acid was confirmed by manganometric titration with potassium manganate(VII).

RESULTS AND DISCUSSION

Photocatalytic Activity. In the first stage of the experiments, the optimum ratio of the silver nanoparticles to titanium oxide was determined. Oxalic acid was chosen as a model compound because of its outstanding stability

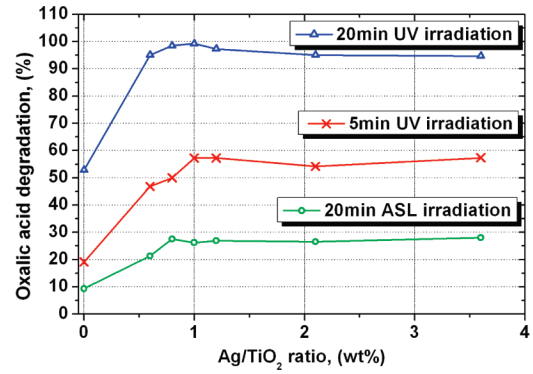

FIGURE 2. Decomposition efficiency for oxalic acid under ASL and UV irradiation for various silver concentration in Ag/P25 composite.

Table 2. Photocatalytic Activity of P25 and Aelected Ag/P25 Composites in Photocatalytic Degradation of Various Contaminants

		pure P25		Ag/P25, 1.0 wt %		Ag/P25, 2.1 wt %	
sample	irradiation time/min	ASL	UV	ASL	UV	ASL	UV
OxA	20	9.3	52.9	26.3	99.2	26.5	95.1
	5		19.2		57.3		54.2
FA	60	0.6	6.6	0.5	14.5	2.1	21.3
HA	60	3.0	34.4	4.1	41.5	3.6	62.7

under both UV and ASL irradiation. Figure 2 shows the dependence of the conversion of OxA in the photocatalytic process on the Ag/TiO_2 ratio in the composite. The effectiveness of OxA decomposition increased rapidly up to a 1.0 wt % Ag/TiO_2 ratio and approached a flat maximum between 0.8 and 1.2 wt %; the effectiveness then stabilized. The shape of curves suggests that 1 wt % silver nanoparticles is high enough to reach optimum photoactivity.

Figure II in the Supporting Information shows the OxA decomposition kinetics. The shape of the curves suggested the Langmuir−Hinshelwood reaction mechanism, which is in good agreement with the results of other works (46, 47). That mechanism is well-known and widely accepted in heterogeneous photocatalysis.

Almost 100% decomposition of oxalic acid has been attained in 20 min when UV radiation was used. The Ag/TiO_2 composite containing at least 1.0 and 2.1 wt % of Ag irradiated by UV light showed about twice as high activity as pure P25 (Table 2). What is even more important is that very high photoactivity for OxA decomposition was also observed under ASL irradiation.

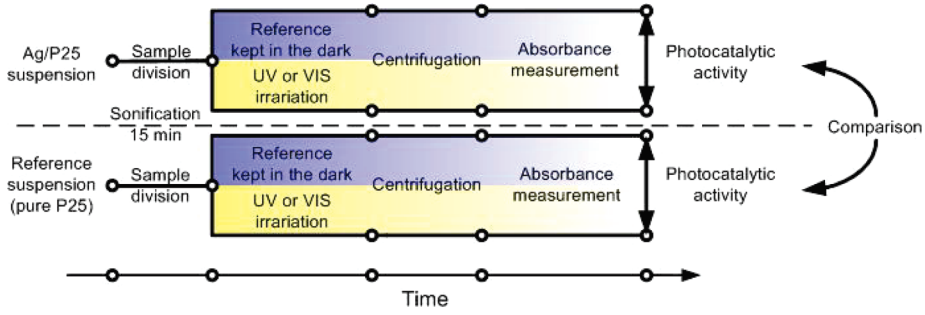

FIGURE 1. Sample preparation to the spectrophotometric measurement.

Table 3. XPS and EDXS Analysis of Ag/P25-2.1 wt % Composite Freshly Synthesized (1), Suspension of Ag/TiO_2 Composite in HA Solution Kept in the Dark (2), Suspension after ASL Irradiation (3), Suspension after UV Irradiation (4)[a]

	Ag $3d_{5/2}$ (A)		Ag $3d_{5/2}$ (B)					
sample	BE (eV)	%	BE (eV)	%	Ag $L_4N_{45}N_{45}$ (eV)	α' (eV)	XPS Ag/Ti	EDXS Ag/Ti
1	367.7	78.2	368.6	21.8	358.4	726.1	0.081	0.018
2	368.0	82.4	369.4	17.6	357.6	725.6	0.096	0.013
3	367.8	93.2	369.2	6.8	358.9	726.7	0.065	0.011
4	367.5	83.7	368.5	16.3	358.4	725.9	0.124	0.015

[a] A, ratio of the intensity of the Ag 3d emission line that may be ascribed to metallic silver; B, ratio of the higher BE component.

To confirm the applicability of spectrophotometric measurements in determination of OxA uptake from the solution, we performed some experiments with the application of manganometric titration. Obtained results showed that spectrophotometric measurements give practically the same results as manganometric titration. The difference between the values of concentration registered for these two measuring techniques was 2.4% for ASL irradiation and 1.1% for UV irradiation.

The same photocatalytic tests as for OxA were performed for formic acid. Significant increase in activity for the Ag-modified sample was observed in the case of UV irradiation (Table 2) for both FA and HA. In the case of ASL irradiation of the composite containing 1.0 and 2.1 wt % Ag, decomposition of FA was practically the same as for the unmodified sample. An increase in silver concentration to 2.1 wt % resulted in some increase of the FA degradation under UV irradiation when compared to 1 wt % Ag.

We found that our Ag/TiO_2 catalyst degrades HA under UV irradiation effectively although its efficiency depends on silver concentration (Table 2). For ASL irradiation, silver addition to TiO_2 does not triggers the HA degradation.

XPS Analysis. The chemical composition of Ag/TiO_2 composite before and after the photocatalytic tests was analyzed by the XPS method (Table 3). The chemical state of silver in the composite was determined by analysis of Ag 3d core excitation and Auger spectrum (XAES). The Ag 3d peaks of all composite samples were slightly asymmetric. Good fit was obtained when two doublets were applied in the spectrum fitting procedure. The electron binding energy (BE) of the most intense peak (A) was found in the range of 367.5−368.0 eV for all studied samples.

The Auger parameter (α' = Ag $3d_{5/2}$ (BE) + Ag $L_4N_{45}N_{45}$ (KE)) showed values above 725 eV. Analysis of Ag $3d_{5/2}$ BE and α' parameters showed that metallic silver is main silver species present in the composite (48). No component that might be ascribed to silver oxide was found in the spectrum (48). Additionally, because the BE of the Ag 3d core excitation depends on the particle size (49, 50), the presence of the second peak at BE of 368.5−369.2 eV in the XPS spectra suggests that part of silver at the TiO_2 surface forms nanoparticles. However, silver forming silver salts with some organic acids may show a similar position of the higher BE component (48).

The XPS analysis allowed calculation of the Ag to Ti atomic ratio (Table 3). The XPS analysis depth for Ag and TiO_2 was estimated to 5.2 and 7.4 nm, respectively (51). The results suggest that irradiation of the composite suspension with either ASL or UV light changes Ag concentration at the titania surface. The highest Ag concentration is observed at the composite surface after UV irradiation (even higher than in the case of as-synthesized sample) contrary to the ASL irradiated one, where the lowest value was obtained. This result was confirmed by EDXS analysis (Table 3) although generally much lower values of the Ag/Ti were found. The EDXS analysis depth is much larger comparing to XPS, it can approach 1 μm. Taking the above into account, the comparison of the results of XPS and EDS analyses shows that Ag clusters/nanoparticles decorated the TiO_2 surface. Further, on the basis of the XPS and EDXS analysis, one can conclude that the ratio of the surface occupied by Ag nanoparticles increases significantly after UV treatment. The following mechanism may explain observed behavior. Silver nanoparticles are surface oxidized and the silver is partially removed from the surface. On the other hand, the presence of organic species causes reduction of Ag^+ ions under UV irradiation and redeposition of silver on the titania surface, which increases the surface area occupied by silver nanoparticles. In the case of ASL irradiation, the reduction process is slower than under UV so the amount of silver on the surface after ASL irradiation is lower than in the case of sample kept in the dark.

SEM and EDXS Analysis. Images a and b in Figure 3 present the SEM images obtained for the Ag/TiO_2 composite containing 1.2 wt % silver nanoparticles. Image a shows morphology of the composite. In Figure 3b, the backscattered electrons (BSE) were used to obtain the SEM image sensitive to the larger atomic number (Z). In this picture, the bright spots were identified as the silver nanoparticles. Most of the Ag particles show rather low diameter (up to 20 nm) although there is a small number of relatively large particles (more then 50 nm). The titanium and silver concentrations in the EDXS analyzed points (Figure 3b) are collected in Table 4. The Ag concentration shows nonuniform distribution over the sample that varies from 1.7 to 5.2 wt %.

TEM and EDXS Analysis. The silver distribution over the Ag/TiO_2 sample was also analyzed by TEM technique. Figure 3c shows the inhomogeneity of the composite morphology and nonuniform size distribution of TiO_2 particles. The images obtained by using HAADF-TEM detector (Figure 3d) where the color brightness is proportional to the Z^2 value,

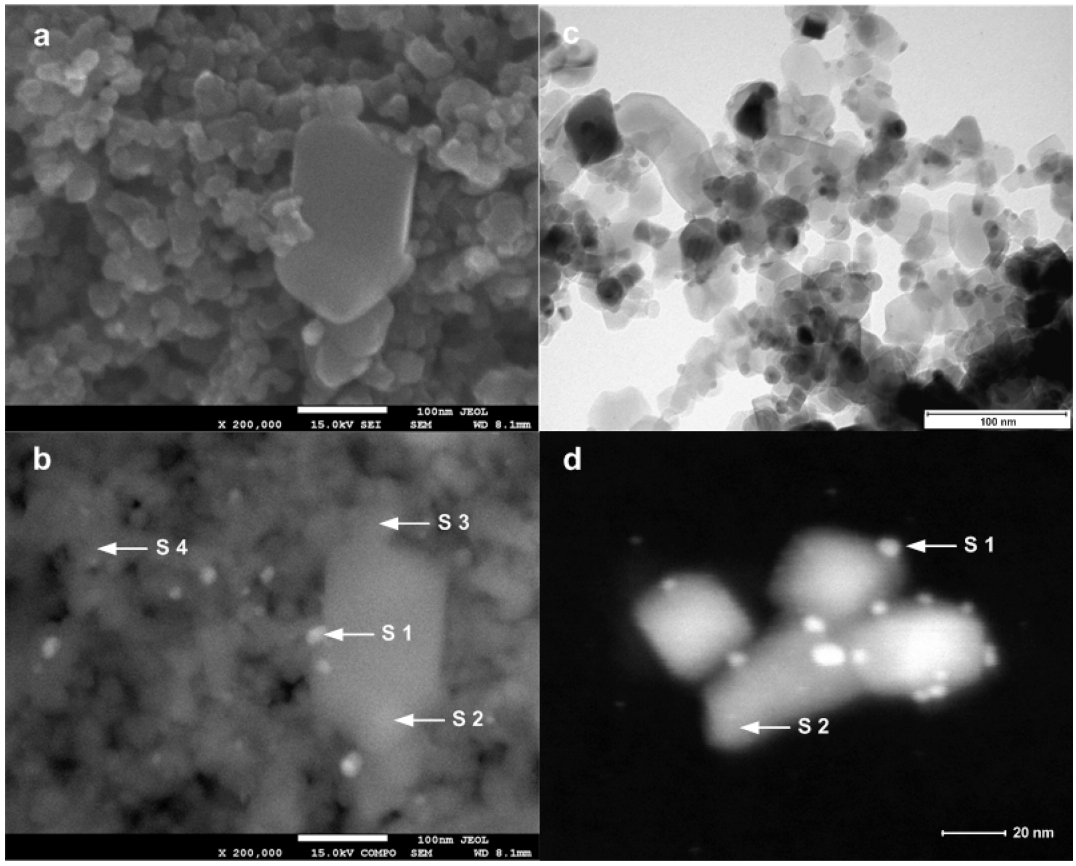

FIGURE 3. (a) SEM and (b) BSE images of Ag/P25 composite (1.2 wt %), (c) TEM and (d) HAADF-TEM images of theAg/P25 composite (2.1 wt %).

Table 4. Distribution of Ag Nanoparticles

	wt %							
spectrum	spectrum 1	spectrum 2	spectrum 3	spectrum. 4	mean	std dev	max	min
Ti	94.8	98.2	98.3	97.7	97.2	1.7	98.3	94.8
Ag	5.2	1.8	1.7	2.3	2.8	1.7	5.2	1.7

showed single spherical Ag nanoparticles with diameter in the range of 4−12 nm. The EDXS analysis confirmed presence of silver as the bright particles (S1; Figure 3d) and that the substrate surface is free of silver outside the places where the Ag particles adhere to the surface (S2; Figure 3d).

DRS and Flat Band Potential Analysis. To describe the spectral properties of obtained composites, we performed DRS measurements. Reflectance spectra were converted to the absorbance spectra using Kubelka−Munk equation (eqs 2 and 3) (52).

$$F(R_\infty(\lambda)) = \frac{(1 - R_\infty)^2}{2R_\infty} \quad (2)$$

$$R_\infty = \frac{R}{R_{BaSO_4}} \quad (3)$$

where R is the reflectance recorded for a sample and R_{BaSO_2} is the reflectance recorder for a reference.

Notice that 2.1 wt % Ag/P25 composites absorb light in the whole visible region, which might suggest that obtained photocatalyst could be active in the visible-light region. Absorption of the visible light by this composite may be explained by surface plasmon resonance effect (SPR). That effect relies on excitation of collective electron oscillations in the metal nanoparticle by the electric field of electromagnetic wave. Magnification of electric field inside and in the nearest neighborhood of a nanoparticle is the direct reason of the appearance of many optical effects. Figure III in the Supporting Information shows absorbance spectra of pure P25 and the 2.1 wt % Ag/P25 composite. An additional absorbance band with a maximum at about 570 nm observed for silver modified photocatalyst may be ascribed to the plasmon effect.

To calculate the band-gap energy, we converted the Kubelka−Munk function to the form $(F(R_\infty)E)^{1/2}$ and changed the wavelength to energy units (eV). Depending on the choice of the method of extrapolation (see Figure 4), different values of band gap energy may be obtained.

Depending on the mode of extrapolation (see Figure 4), that method gives an ambiguous value of band-gap energy

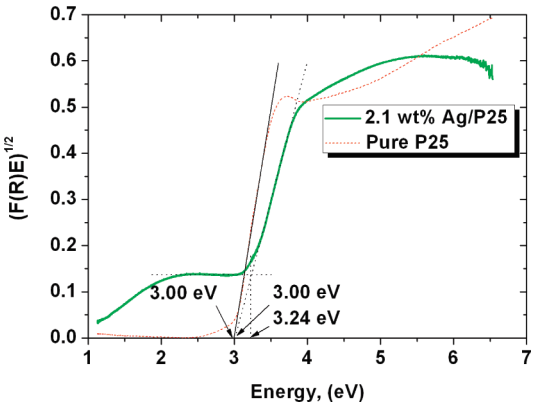

FIGURE 4. Determination of the band gap energy values for pure P25 TiO_2 and TiO_2 -modified with Ag nanoparticles (2.1 wt % Ag/P25 composite).

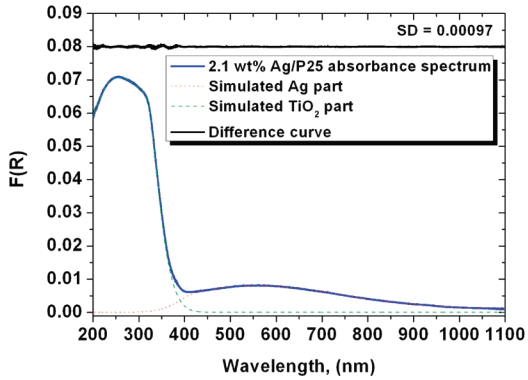

FIGURE 5. Simulated shape of TiO_2 part and Ag part as well their sum fitted to the spectrum registered for the 2.1 wt % Ag/P25 composite. The difference between the simulated and measured spectrum is shown too.

charged by relatively high error. The authors offer another solution, which uses additivity properties of absorbance spectra obtained by Kubelka–Munk conversion. Thirteen additive components were fitted to the contour of absorbance spectrum of silver composite using CasaXPS (ver. 2.3.12) program. The sum of 7 peaks was assigned to the titanium dioxide spectrum and the sum of the other 6 peaks to the silver spectrum. The simulated envelop was compared with absorbance spectrum of the composite. Standard deviation was calculated to check fitting quality (Figure 5).

After that, the TiO_2 part of the composite spectrum was transformed to the $(F(R)E)^{1/2}$ form and compared with the similarly converted pure P25 spectrum. In consequence value of band-gap energy was obtained (see Figure 6). That method of calculating band-gap energy gives highly probable results charged by lower error than the previously described one. Note that such measured band-gap energy for the composite was practically identical to that of a pure P25 TiO_2.

Flat band potential was measured for pure P25 and 2.1 % Ag/P25 composite. Both measurements were repeated at least three times. Determination of conduction band edge energy was carried out using following equation

$$E_{CB}(\mathrm{pH}) \cong E^0_{MV^{2+/+\bullet}} + k(\mathrm{pH}_0 - \mathrm{pH}) \qquad (4)$$

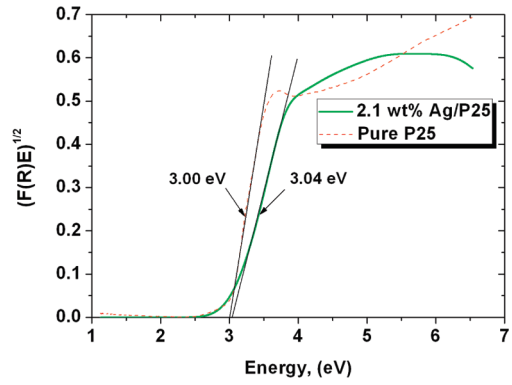

FIGURE 6. Comparison of the band gap energy values for pure P25 and simulated TiO_2 part of the spectrum for the 2.1 wt % Ag/P25 spectrum.

Table 5. Location of E_{CB} and E_{VB} for Pure P25 and 2.1 wt % Ag/P25 Composite for pHs Values Measured in the Suspensions Containing Various Contaminants

					vs Ag/AgCl	
material	substrate	suspension pH	pH_0	E_{bg} (eV)	E_{CB} (V)	E_{VB} (V)
pure P25		0	5.96 ± 0.15	3.00	−0.09	2.91
	OxA	3.36			−0.29	2.71
	FA	2.63			−0.25	2.75
	HA	6.55			−0.48	2.52
2.1 wt % Ag/P25		0	5.98 ± 0.10	3.04	−0.09	2.95
	OxA	3.47			−0.30	2.74
	FA	2.63			−0.25	2.79
	HA	6.54			−0.48	2.56

where E_{CB} is conduction band edge energy, $E^0_{MV^{2+/+\bullet}} = 0.445$ V is methylviologen redox potential, k is a coefficient defining the E_{CB} change caused by unit pH change (for TiO_2, $k = 0.059$ V), pH_0 is the pH value when $E_{CB} = E^0_{MV^{2+/+\bullet}}$, and pH is suspension pH.

The pH_0 value was determined from inflection point as an average of marked point on the graphs (see Figure IVa-b in the Supporting Information).

Values of conduction band edge energy were calculated for pH of zero and for suspension pHs (Table 5).

Obtained values of pH_0 for both photocatalysts were practically the same, which is in accordance with literature data (53, 54). Oxidation potentials of the OxA (+0.91 V) and FA (+0.87 V) were determined by the CV and are located in the band-gap region of TiO_2. It was impossible to measure HA oxidation potential because it is a mixture of different compounds.

BET Analysis. The surface area obtained for 2.1 % Ag/P25 (49.4 m^2/g) was smaller than for pure P25 (56.6 m^2/g). Probably silver nanoparticles are deposited in the cracks and holes of agglomerates of TiO_2. It suggests that the composite photoactivity was created only by synergic effect between Ag nanoparticle and P25 that overcomes the observed effect of the specific surface area decrease.

In general, the studied system shows outstanding catalytic activity in the ultraviolet light region. Under ASL irradiation silver composites showed high activity only in the photodegradation of OxA.

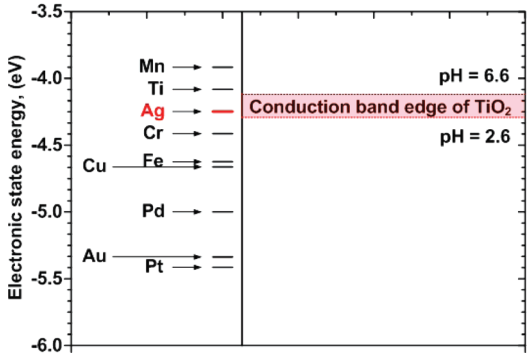

FIGURE 7. Comparison between the position of the Fermi level of selected metals and location of the TiO_2 conduction band at the potential of zero charge at different pH on the electronic state energy scale.

The observed silver composite activity could be explained by the fact that silver occupies an exceptional position among metals from the point of view of its electronic properties. The work function of silver is much lower than the work function of other noble metals, especially gold and platinum, and even lower than the work function of some common metals like iron or nickel (see Figure 7).

At the same time, silver is relatively resistive to dissolution: the normal potential of the reaction $Ag^+ + e^- = Ag^0$ is much higher than the respective potentials of the common metals and not much lower than of other noble metals. So, metallic silver at the TiO_2 surface can resist the attack of oxidizing agents from the solution or, vice versa, oxidized silver is a strong oxidizer. The usual explanation for the enhanced activity of the Pt or Au loaded TiO_2 is the formation of so-called Schottky barrier at the surface TiO_2/metal. The Fermi level of those metals is situated deeply below the conduction band edge of TiO_2 (see Figure 7) and the electrons can flow in one direction only, from TiO_2 to metal (53, 54). At the metal surface they are consumed in a reaction of hydrogen evolution or oxygen reduction. So, the metal particles deposited at the TiO_2 surface becomes traps for electrons, facilitating the process of charge separation in the photocatalytic process. In the case of silver, the Fermi level of the metal is situated close to the conduction band edge of TiO_2, and no Schottky barrier can be formed. So, electrons can flow in both directions, enabling the capture of a hole by the silver particle.

According to the literature, the decomposition of OxA on bare TiO_2 surface proceeds probably according to the following mechanism (55, 56)

After excitation of TiO_2 with light of energy higher than that of the band gap, electron−hole pairs are formed. The photoinduced carriers migrate to the surface of the particles where they take part in redox reactions. Holes oxidize water or surface hydroxyls, whereas electrons reduce dissolved oxygen (eq 1).

$$TiO_2(h^+_{vb}) + HO^-_{(ads)} \rightarrow TiO_2 + OH^{\bullet}_{(ads)} \quad (1)$$

$$TiO_2(e^-_{cb}) + O_{2(ads)} + H^+ \rightarrow TiO_2 + HO_2^{\bullet} \leftrightarrow O_2^{\bullet -} + H^+ \quad (2)$$

$$2\ HO_2^{\bullet} \rightarrow H_2O_2 + O_2 \quad (3)$$

$$H_2O_2 + e^-_{cb} \rightarrow OH^{\bullet} + OH^- \quad (4)$$

From both reactions 1 and 4, strong oxidizing hydroxyl radicals are generated, which may in turn attack organic contaminants like oxalate species (55)

$$HOOC\text{-}COO^- + OH^{\bullet} \rightarrow HOOC\text{-}COO^{\bullet} + OH^- \quad (5)$$

$$HOOC\text{-}COO^{\bullet} \rightarrow CO_2^{\bullet -} + CO_2 + H^+ \quad (6)$$

$$HOOC\text{-}COO^{\bullet} + O_2 \rightarrow HO_2^{\bullet} + 2CO_2 \text{ (in the presence of oxygen)} \quad (7)$$

Another possibility is the direct oxidation of the organic species by holes

$$HOOC\text{-}COO^- + h^+_{vb} \rightarrow HOOC\text{-}COO^{\bullet} \quad (8)$$

In the case of Ag/TiO_2 composites, the photodegradation mechanism may proceed in two ways. In the presence of hydrogen peroxide, which is formed in accordance with equation 3, silver nanoparticles are surface oxidized (56)

$$Ag^0_{(nano)} + H_2O_2 + H^+ \rightarrow Ag^+_{(surf.\ or\ susp.)} + OH^{\bullet} + H_2O \quad (9)$$

Ag^+ ions stay on the silver nanoparticle or they move into the solution. In the latter case, Ag^+ cations react with $HC_2O_4^-$ anions and adsorb on the surface (eqs 8 and 9). $HC_2O_4^-$ anions stand for 85% of oxalate species present in solution at this reaction condition (pH 3.5), which suggests that route of oxidation process.

$$Ag^+_{(susp)} + HOOC\text{-}COO^- \rightarrow HOOC\text{-}COOAg_{(TiO2\ or\ Ag\ surf.)} \quad (10)$$

After that process, adsorbed $HC_2O_4^-$ anions are oxidized under the influence of hydroxyl radicals, which are produced in the reaction of direct photoexcitation of TiO_2 (eq 10)

$$HOOC\text{-}COOAg_{(TiO2\ or\ Ag\ surf.)} + OH^{\bullet} \rightarrow HOOC\text{-}COO^{\bullet} + OH^- + Ag^+ \quad (11)$$

Reduction of Ag cations occurs with the participation of carboxyl anion radicals created in the reaction *6* or photogenerated electrons (see eq 12).

$$Ag^{+}_{(TiO2\ or\ Ag\ surf)} + CO_2^{\bullet -} \rightarrow Ag^{0}_{(nano)} + CO_2 \qquad (12)$$

$$Ag^{+}_{(TiO2\ or\ Ag\ surf)} + e^{-}_{cb} \rightarrow Ag^{0}_{(nano)} \qquad (13)$$

Oxidation of silver nanoparticles is also possible by the holes generated in the valence band (see eq 13). After that process, the oxalate oxidation cycle starts again according to equation 14.

$$Ag^{0}_{(nano)} + TiO_2(h^{+}_{vb}) \rightarrow Ag^{+}_{(Agnano)} + TiO_2 \qquad (14)$$

However, such a mechanism is possible only in the case of UV irradiation. In the case of ASL irradiation, such a mechanism is impossible, because the condition for its occurrence is the generation of the $OH^{\bullet}$ radicals (reaction 4). In our precise measurements, we have shown that the band gap of TiO_2 in the Ag/TiO_2 composite is exactly the same as in the case of pure TiO_2. Note that in the case of similar compounds, formic acid composite showed no activity. The possible explanation may be found by invoking the properties of silver oxalate. That compound is sensitive to visible light and decomposes under its influence. So, when the adsorbed complex of oxalate anion on the Ag surface is formed, it may also be sensitive to visible light and can decompose under its influence, according to the following reaction

$$HOOC\text{-}COOAg_{(surf)} \xrightarrow{h\nu} HOOC\text{-}COO^{\bullet} + Ag^{\bullet} \qquad (15)$$

$$HOOC\text{-}COO^{\bullet} + H_2O \rightarrow H_2C_2O_4 + OH^{\bullet} \qquad (16)$$

Note that the transfer of electrons from silver to TiO_2 with the creation of positive charge on the surface of silver would facilitate adsorption of oxalate anion on the surface of silver. Such transfer is very probable in view of the presented position of the Ag Fermi level versus TiO_2 band edges.

CONCLUSION

The synthesized Ag/P25 composites containing various concentrations (0.6−3.7 wt %) of the silver nanoparticles on the titania surface were tested as a potential photocatalyst to remove organic contaminations from water. It was proved that a small amount of silver nanoparticles (1 wt %) greatly increase photocatalytic activity of TiO_2. The Ag/P25 composite showed oxidation activity significantly higher than pure P25 in the case of OxA, FA, and HA under UV irradiation. In the degradation reaction of OxA, under ASL irradiation, silver composites were several times more active than pure P25. XPS analysis proved the presence of metallic silver as the main silver component of the silver nanoparticle both in as-synthesized composites as well as after the reaction. Furthermore, in the presence of organic substances and UV irradiation, surface occupied by silver nanoparticles developed what is connected with partial oxidation of deposited silver nanoparticles with subsequent reduction. The TEM measurements showed spherically shaped Ag particles whose sizes were in the range 4−12 nm. An analysis of the electrochemical properties of the obtained composites proved that silver kept the location of conduction band energy and band-gap energy unchanged. According to the opinion of the authors, the high activity of Ag/TiO_2 composite may be ascribed to the unusual electronic properties of silver.

Acknowledgment. The authors thank Dr. Wojciech Macyk for fruitful discussion and Dr. Lidia Lityńska for TEM measurements. This research was supported by European Economic Area Financial Mechanism, Grant PL0084 (2007−2010) NOMRemove: Effective photocatalytic-membrane methods of removal of organic contaminants for water treatment.

Supporting Information Available: Additional figures (PDF). This material is available free of charge via the Internet at http://pubs.acs.org.

REFERENCES AND NOTES

(1) Carp, O.; Huisman, C. L.; Reller, A. *Prog. Solid State Chem.* **2004**, *32*, 33–177.
(2) Hoffmann, M. R.; Martin, S. T.; Choi, W.; Bahnemann, D. W. *Chem. Rev.* **1995**, *95*, 69–96.
(3) Sivalingam, G.; Nagaveni, K.; Hegde, M. S.; Madras, G. *Appl. Catal., B* **2003**, *45*, 23–38.
(4) Hu, C.; Tang, Y.; Jiang, Z.; Hao, Z.; Tang, H.; Wong, P. K. *Appl. Catal., A* **2003**, *253*, 389–396.
(5) Chiang, K.; Lim, T. M.; Tsen, L.; Lee, C. C. *Appl. Catal., A* **2004**, *261*, 225–237.
(6) Coleman, H. M.; Chiang, K.; Amal, R. *Chem. Eng. J.* **2005**, *113*, 65–72.
(7) Zhang, Z.; Wang, C.; Zakaria, R.; Ying, J. Y. *J. Phys. Chem. B* **1998**, *102*, 10871–10878.
(8) Arana, J.; Dona-Rodriguez, J. M.; Gonzalez-Diaz, O.; Tello Rendon, E.; Herrera Melian, J. A.; Colon, G.; Navio, J. A.; Perez Pena, J. *J. Mol. Catal., A* **2004**, *215*, 153–160.
(9) Ohtani, B.; Iwai, K.; Nishimoto, S.; Sato, S. *J. Phys. Chem. B* **1997**, *101*, 3349–3359.
(10) Haibin, L.; Xuechen, D.; Guocong, L.; Xiaoqi, L. *J. Mater. Sci.* **2008**, *43*, 1669–1676.
(11) Egerton, T. A.; Mattinson, J. A. *J. Photochem. Photobiol., A* **2008**, *194*, 283–289.
(12) Gao, Y. M.; Lee, W.; Trehan, R.; Kershav, R.; Dwight, K.; Wold, A. *Mater. Res. Bull.* **1991**, *26*, 1247–1254.
(13) Herrmann, J. M.; Disdier, J.; Pichat, P.; Fernandez, A.; Gonzalez-Elipe, A.; Munuera, G.; Leclercq, C. *J. Catal.* **1991**, *132*, 490–497.
(14) Young, C.; Lim, T. M.; Chiang, K.; Scott, J.; Amal, R. *Appl. Catal., B* **2008**, *78*, 1–10.
(15) Nazeeruddin, M. K.; Kay, A.; Rodicio, I.; Humphry Baker, R.; Muller, E.; Liska, P.; Vlachopoulos, N.; Grätzel, M. *J. Am. Chem. Soc.* **1993**, *115*, 6382–6390.
(16) Cherepy, N. J.; Smestad, G. P.; Grätzel, M.; Zhang, J. Z. *J. Phys. Chem. B.* **1997**, *101*, 9342–9351.
(17) O'Regan, B.; Grätzel, M. *Nature* **1991**, *353*, 737–739.
(18) Lanata, M.; Cherchi, M.; Zappettini, A.; Pietralunga, S. M.; Martinelli, M. *Opt. Mater.* **2001**, *17*, 11–14.
(19) Fujishima, A.; Honda, K. *Nature* **1972**, *238*, 37–38.
(20) Li, F. B.; Li, X. Z. *Chemosphere* **2002**, *48*, 1103–1111.
(21) Zhang, F.; Jin, R.; Chen, J.; Shao, C.; Gao, W.; Li, L. *J. Cat.* **2005**, *232*, 424–431.

(22) Qi, X. H.; Wang, Z. H.; Zhuang, Y. Y.; Yu, Y.; Li, J. L. *J. Hazard. Mater.* **2005**, *118*, 219–225.
(23) Sakthivel, S.; Shankar, M. V.; Palanichamy, M.; Arabindoo, B.; Bahnemann, D. W.; Murugesan, V. *Water Res.* **2004**, *38*, 3001–3008.
(24) Vamathevan, V.; Amal, R.; Beydoun, D.; Low, G.; McEvoy, S. *J. Photochem. Photobiol., A* **2002**, *148*, 233–245.
(25) Robertson, P. K. J.; Bahnemann, D. W.; Robertson, J. M. C.; Wood, F. *Handbook of Environmental Chemistry*; Springer: Heidelberg, Germany, 2005; Vol. 2, part M, p 367—423.
(26) Li, Q.; Mahendra, S.; Lyon, D. Y.; Brunet, L.; Liga, M. V.; Li, D.; Alvarez, P. J. *J. Water Res.* **2008**, *42*, 4591–4602.
(27) Linsebigler, A. L.; Lu, G.; Yates, J. T. *Chem. Rev.* **1995**, *95*, 735–758.
(28) Hofmann, M. R.; Martin, S. T.; Choi, W.; Bahnemann, D. W. *Chem. Rev.* **1995**, *95*, 69–96.
(29) Mills, A.; Le Hunte, S. *J. Photochem. Photobiol., A* **1997**, *108*, 1–35.
(30) Kiriakidou, F.; Kondarides, D. I.; Verykios, X. E. *Catal. Today* **1999**, *54*, 119–130.
(31) Sobana, N.; Selvam, K.; Swaminathan, M. *Sep. Purif. Technol.* **2008**, *62*, 648–653.
(32) Li, H.; Duan, X.; Liu, G.; Liu, X. *J. Mater. Sci.* **2008**, *43*, 1669–1676.
(33) Li, Ch.; Hsieh, Y.; Chiu, W.; Liu, Ch.; Kao, Ch *Sep. Purif. Technol.* **2007**, *58*, 148–151.
(34) Hou, X.; Huang, M.; Wu, X.; Liu, A. *Chem. Eng. J.* **2009**, *146*, 42–48.
(35) Nakata, K.; Udagawa, K.; Tryk, D. A.; Ochiai, Y.; Nishimoto, S.; Sakai, H.; Murakami, T.; Abe, M.; Fujishima, A. *Mater. Lett.* **2009**, *63*, 1628–1630.
(36) Paramasivam, I.; Macak, J. M.; Ghicov, A.; Schmuki, P. *Chem. Phys.Lett.* **2007**, *445*, 233–237.
(37) Li, H.; Duan, X.; Liu, G.; Liu, X. *J. Mater. Sci.* **2008**, *43*, 1669–1676.
(38) Wang, K. H.; Hsieh, Y. H.; Chao, P. W.; Chang, C. T. *J. Hazard. Mater.* **2002**, *95* (1—2), 161–174.
(39) Kubacka, A.; Ferrer, M.; Martinez-Arias, A.; Fernandez-Garcia, M. *Appl. Catal., B* **2008**, *84*, 87–93.
(40) Lai, Y.; Chen, Y.; Zhuang, H.; Lin, Ch *Mater. Lett.* **2008**, *62*, 3688–3690.
(41) Malagutti, A. R.; Mourao, H.A.J. L.; Garbin, J. R.; Ribeiro, C. *Appl. Catal., B* **2009**, *l90*, 205–212.
(42) Wodka D.; Nowak P.; Warszyński P.; Kumakiri I.; Simon C. *XLI Polish Annual Conference on Catalysis*, Krakow, Poland, March 30—April 1, 2010; Institute of Catalysis and Surface Chemistry PAS: Krakow, Vol. 22, p 39.
(43) Stevenson, F. J. *Humus Chemistry: Genesis, Composition, Reactions*; John Wiley and Sons, New York, 1994.
(44) Goel, S.; Hozalski, R. M.; Bouwer, E. J. *J. Am. Water Works Assoc.* **1995**, *87* (1), 90–105.
(45) Roy, A. M.; De, G. C.; Sasmal, N.; Bhattacharyya, S. S. *Int. J. Hydrogen Energy* **1995**, *20* (8), 627–630.
(46) Kosanic, M. M. *J. Photochem. Photobiol., A* **1998**, *119*, 119–122.
(47) MacMurray, T. A.; Byrne, J. A.; Dunlop, P. S. M.; Winkelman, J. G. M.; Eggins, B. R.; McAdams, E. T. *Appl. Catal., A* **2004**, *262*, 105–110.
(48) *NIST X-ray Photoelectron Spectroscopy Database*; National Institute of Standards and Technology: Gaithersburg, MD; http://srdata.nist.gov/xps/.
(49) Shin, H. S.; Choi, H.Ch.; Jung, Y.; Kim, S. B.; Song, H. J.; Shin, H. J. *Chem. Phys. Lett.* **2004**, *4383*, 18–422.
(50) Lim, D.Ch.; Lopez-Salido, I.; Kim, Y. D. *Surf. Sci.* **2005**, *598*, 96–103.
(51) Tanuma, S.; Powell, C. J.; Penn, D. R. *Surf. Interface Anal.* **1993**, *21*, 165.
(52) Kortüm, G. *Reflectance Spectroscopy*; Springer-Verlag: Berlin, 1969; p 180.
(53) Morrison, S. R. *Electrochemistry at Semiconductor and Oxidized Metal Electrodes*; Plenum Press: New York, 1980; p 183.
(54) Bard, A. J. *Standard Potentials in Aqueous Solution*, 2nd ed.; Parsons, R., Jordan, J., Eds.; Marcel Dekker: New York, 1985; p 36.
(55) Quici, N.; Morgada, M. E.; Piperata, G.; Babay, P.; Gettar, R. T.; Litter, M. I. *Catal. Today* **2005**, *101*, 253–260.
(56) Litter, M. I. *Appl. Catal., B* **1999**, *23*, 89–114.

AM1002684